CORRELATIVE MICROSCOPY AND SPECTROSCOPY OF PEROVSKITE THIN FILMS: DEGRADATION ANALYSIS

V.Paraskeva[1], E. Peraticos[1], S. Pechmann[2,3], T. Fontanot[2,3], A. Aguirre[4,5,6], T. Aernouts[4,5,6], A. Krishna[4,5,6], M. Hadjipanayi[1], M. Sergides[7], A. Othonos[7], S. Christiansen[2,3], R. Ebner[8], G.E. Georghiou[1]
[1]University of Cyprus, PV Technology Laboratory, Department of Electrical & Computer Engineering, Nicosia, Cyprus
[2]Fraunhofer IKTS, Fraunhofer Institute for Ceramic Technologies and Systems, Äußere Nürnberger Str. 62, 91301 Forchheim, Germany
[3]Max-Planck-Institut für die Physik des Lichts, 91058 Erlangen, Germany
[4]Imec, imo-imomec, Thin Film PV Technology – partner in Solliance, Thor Park 8320, 3600 Genk, Belgium
[5]EnergyVille, imo-imomec, Thor Park 8320, 3600 Genk, Belgium
[6]Hasselt University, imo-imomec, Martelarenlaan 42, 3500 Hasselt, Belgium
[7]Laboratory of Ultrafast Science, Department of Physics, University of Cyprus, Nicosia, 1678, Cyprus
[8]AIT Austrian Institute of Technology, Center for Energy, Giefinggasse 2, 1210 Vienna, Austria

ABSTRACT: Perovskite materials have excellent prospects for semiconducting applications due to their desirable photoelectric properties. The morphology and the structure of the light absorption layer are crucially important for the device performance and their changes through the degradation period are of upmost importance for understanding degradation pathways. In this work, pristine perovskite thin films with and without FACl additives in the active perovskite layer have been characterized with Scanning Electron Microscopy (SEM), Atomic Force Microscopy (AFM) and Energy-Dispersive Spectroscopy (EDX) to identify changes in the perovskite grain size, grain boundaries and current densities. Moreover, femtosecond transient transmission measurements have been employed to detect changes in carrier relaxation dynamics in encapsulated perovskite thin films before and after outdoor exposure.
Keywords: perovskites, microscopy, spectroscopy

1 INTRODUCTION

Perovskite solar cells have demonstrated outstanding performance in recent years, achieving power conversion efficiencies (PCE) as high as 25.5% with theoretical efficiencies calculated up to 31% [1]. A lot of indoor characterization testing was implemented the last years at different temperatures, humidity levels, bias loading demonstrating the impact of each parameter on the perovskite lifetime and stability [2]. Understanding the degradation pathways of perovskite materials is crucial to improve their stability and pave their way to commercialization. To achieve this, understanding of the fundamental material properties is required through the utilization of advanced microscopic and spectroscopic techniques. Device engineering, morphology, and light-harvesting properties of the perovskite material are the key factors which help to improve the efficiency of perovskite solar cells [3]. Measurement results from those methods can be utilized to understand the long-term outdoor operation of devices and their degradation mechanisms.

Methods of scanning electron microscopy (SEM), and conductive Atomic Force Microscopy (c-AFM) provide information regarding the understanding of the fundamental properties of perovskite materials and solar cells at the nanoscale. One common use of the SEM method is to identify changes in the perovskite grain size and grain boundaries. Grain boundaries are considered detrimental to the performance of the perovksites and modify the charge carrier trasport pathway in the material and hence the performance of perovskites [4]. c-AFM was widely used in the past to characterize the local electrical properties of perovskite thin films [5]. c-AFM gives also valuable conductivity results of grains and grain boundaries as the SEM method which are very helpful for increasing the performance and stability of perovskite-based devices [6].

Energy-Dispersive X-Ray Spectroscopy is used to provide elemental composition details about the speciment under test. It is typically used concurrently with image acquistion in order to confirm that the specimen is composed of the expected elements and that these have the expected stoichiometric ratio.

Ultrafast pump-probe spectroscopy provides a powerful approach for deep insight into the transient photophysics of electron-hole interactions. Correlation between carrier dynamics and aging of the device was found in the past providing an insight into the factors driving degradation in perovskite solar cells [7].

In this work microscopic investigation of pristine perovskite thin films of two different compositions has been performed using Scanning Electron Microscopy (SEM), Energy Dispersive X-Ray Spectroscopy (EDX) and Atomic Force Microscopy (AFM and c-AFM) to identify differences in their grain sizes and conductive currents. At the same time, fully-fuctional devices with the same perovskite layer were exposed outdoors for investigation of their long-term operation and understanding of their outdoor behavior based on their morphology and photocurrent investigated with the above-mentioned methods. Moreover, Ultrafast spectroscopy has been applied in encapsulated perovskite thin films before and after outdoor testing to reveal changes in carrier dynamics during the outdoor exposure of samples.

2 EXPERIMENTAL APPROACH

2.1 Microscopic measurements (SEM, AFM, EDX)

Several perovskite thin films (i.e., no encapsulation, only active layer deposited on a silicon substrate) were provided to Fraunhofer IKTS for structural characterization. Two different types of samples have been utilized labelled as type A and type B perovskite. Type A perovskite has a perovskite composition $Cs_{0.18}FA_{0.82}PbI_{20.82}Br_{0.18}$ while type B has a perovskite composition of $Cs_{0.1}FA_{0.9}PbI_{2.865}Br_{0.135}$ (+ 5mol% excess of FA and Cl).

During microscopy measurements all samples were cut to smaller pieces to always examine a pristine surface

that has not been altered by exposure to probes from other methods such as electrons or photons. The samples were handled with great care in inert atmosphere to avoid uncontrolled degradation from exposure to moisture and air. Sample transport between the different instruments and the glovebox was also conducted under inert conditions via a special transfer of modules (see Figure 1).

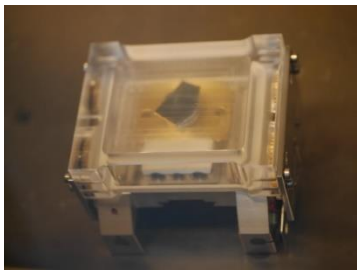

Figure 1: Sample mounted in vacuum shuttle for analysis in Zeiss SEM.

For surface and cross section SEM a Zeiss Crossbeam 550 SEM system was utilized. The system is equipped with a focused ion beam (FIB) for material ablation and cross-section preparation and an energy dispersive X-ray spectrometer (EDX) for element analysis. Images have been acquired exploiting different type of detectors (in-lens detector, secondary electrons detector) and different accelerating voltages (5, 10, 20 kV). The EDX detector (Ultim Max, Oxford Instruments, Abingdon on Thames, UK) was operated with 20 kV electron beam voltage to detect signal from heavier elements according to the perovskite composition. The AFM used was a NX20, manufactured by Park System (Suwon, South Korea), which was exploited to scan the surface of the samples acquiring 2D images to study the morphology and the local conductivity of the sample surface. The measurements were conducted in non-contact mode using a NanoWorld® Arrow™ NCR probe having a tip radius of curvature of less than 10 nm.

2.2 Ultrafast pump-probe spectroscopy

For the spectroscopic investigation of samples, several encapsulated perovskite thin films have been provided to the Laboratory of Ultrafast Science at University of Cyprus. Perovskite thin films consist by only the perovskite layer and this structure was selected for those type of measurements since complete solar cells modules consist of various layers of materials and this makes impossible to understand the complicated ultrafast dynamics in these samples. Ultrafast measurements have been conducted before and after outdoor exposure of the perovskite thin films. The experimental apparatus utilized for those measurements consisted of a Ti:Saphire ultrafast amplifier producing 100 fs pulses centred at 800 nm at a repetition rate of 1 KHz. The pump wavelength at 400 nm was generated using a BBO non-linear crystal. A small part of the fundamental energy (~2.5 μJ) was used to generate white light continuum using a 4 mm sapphire window. This white light was used in probing different energy states in the VIS region of the spectrum between 420 nm to 780 nm.

2.3 Outdoor apparatus

Fully-functional devices with the same perovskite composition used in the microscopy and spectroscopy measurements have been provided to FOSS Research Centre for Sustainable Energy for outdoor testing and investigation of performance degradation outdoors. Comparison of the outdoor degradation of devices with the information provided by the microscopy/spectroscopy techniques is then implemented. During the outdoor testing, the perovskite devices have been located at fixed plane array and current-voltage (I-V) measurements have been collected at regular intervals over several weeks of testing. Forward and reverse voltage sweeps have been applied during each IV curve. Between IV scans, the modules were kept at open-circuit voltage (V_{oc}). The voltage sweep rate was chosen to be 1 V/s while a forward-first voltage sweep strategy has been used in all instances. The outdoor testing of the samples started on the 12th of January 2021 and lasted for 16 weeks. Alongside the I-V traces from the devices, environmental sensors have been used to collect solar irradiance in the plane of array, ambient and device temperature, wind velocity and humidity/precipitation levels.

3 RESULTS & DISCUSSION

3.1 SEM measurements

Surface SEM measurement analysis yields information on the film homogeneity and morphology. All films appear densely packed and cover the whole surface homogeneously. Different grain sizes for the different perovskite types are clearly determined, with a mean diameter of 128 nm (perovskite A) versus 192 nm (perovskite B). The SEM images of the two different types of samples are depicted in Figure 2. According to the literature larger grains were found to exhibit improved photovoltaic properties.

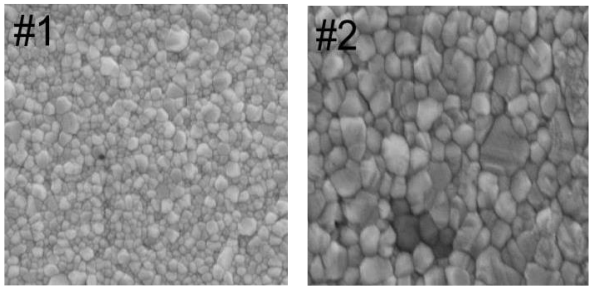

Figure 2: Top view SEM images for perovskite type A (#1) and perovskite type B (#2).

Cross-section SEM was conducted next to have a closer look into the layer interface in order to check adhesion, layer thickness and composition variations. A fractured edge method was utilized for cross-section preparation but this method exhibited mechanical damage on the samples.

3.2 EDX measurements

The elemental composition of the samples was determined via EDX analysis performed on the sample cross-section. Therefore, the whole cross-section was mapped. The EDX elemental map of perovskite type A with composition $Cs_{0.18}FA_{0.82}PbI_{20.82}Br_{0.18}$ is depicted in

Figure 3. The perovskite films show for both samples the expected element composition (Cs, Pb, I, Br, C and N from FA), which is equal for perovskites A and B. Fluor from the added FACl and LiF is detected in type B perovskite as well as Indium and Oxygen from the ITO surface layer. Also, the underlying silicon substrate can be identified. Elemental maps have shown that elements were distributed homogeneously in the perovskite thin films, which confirms that they are of good quality.

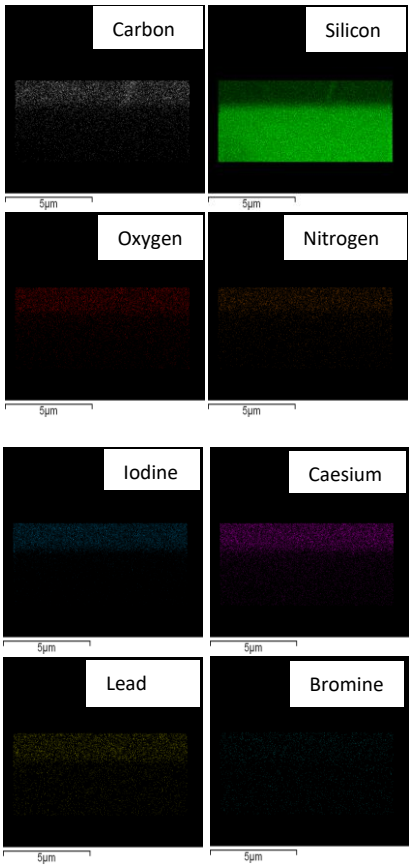

Figure 3: EDX elemental maps of perovskite type A. The perovskite composition of this sample is $Cs_{0.18}FA_{0.82}PbI_{20.82}Br_{0.18}$.

3.3 Atomic Force Microscopy

Height scans of the two different types of perovskites were implemented first (Figure 4). From the topographic images shown in Figure 4, a homogenous coverage and film morphology can be inferred. The grain size distributions fit to the observations from SEM. For perovskite B, a lot of grains apparently contain 2D-defects such as twin boundaries. The average roughness derived from the scanned area calculates to ~7nm and ~15nm for perovskite A and B, respectively.

The film thickness was measured at a film edge prepared by gently scratching with a razor blade. After image processing (slope correction), the histogram is used for thickness determination (see right part of Figure 4). The distance between the background/substrate peak and the film yields the average film thickness; ~470nm for perovskite A and ~610nm for perovskite B.

Conductive Atomic Force Microscopy (c-AFM) is a special AFM mode, which provides information on the electronic properties (local current inhomogeneities coupled to topography) by measuring in contact mode and applying

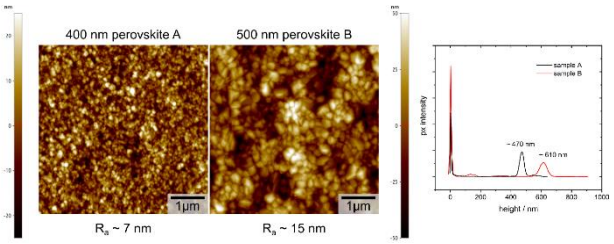

Figure 4: Left: overview AFM height scans of samples A and B in an area of 5x5µm. Right: pixel histogram derived from AFM edge scans to determine the average film thicknesses.

a bias to the sample. The signal is thereby generated by the current flow between the tip and its contact point to the sample. Additionally, the topography is recorded by deflection of the cantilever. Both images are correlated afterwards. For the investigated perovskite samples (A and B, without additional layers on top), perovskite B with its larger grains and less grain boundaries exhibits considerably higher current densities than perovskite A (mean value of 4.1 nA for perovskite B compared to 2.9 nA for perovskite A). Grain boundaries are clearly visible in the c-AFM images, hence, impact the optoelectronic properties. The c-AFM images are depicted in Figure 5.

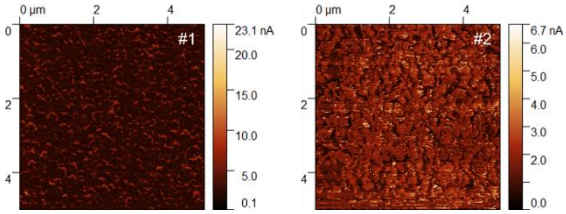

Figure 5: AFM current image of perovskites A (#1) and B (#2). The applied sample bias is -2/2 V.

3.4 Ultrafast spectroscopy

Ultrafast time-resolved differential transmission spectra were obtained for the samples using a continuous of probing wavelengths ranging from 420 nm – 780 nm at room temperature. Samples of perovskite type A were studied with this technique. Initially, femtosecond differential transmission measurements were conducted at pristine samples and at different fluence values (see Figure 6 for the spectra at pump powers 1 µJ). In particular, fluence was varied between 100 µJ/cm^2 and 400 µJ/cm^2. The spectra showed a dominant peak centred at 740 nm. Two additional peaks at 720 nm and 755 nm were also observed. A possible reason for these side-peaks is the presence of defect states energetically located close to the main 740 nm peak. Additionally, negative differential transmission values between 530 nm - 660 nm were observed indicating free carrier absorption. Carriers in this energy range were absorbed by the sample. Eventually, the system evolved to equilibrium. The behavior of the material was not affected by the different pump powers as all spectra obtained present the same features at the different pump powers studied.

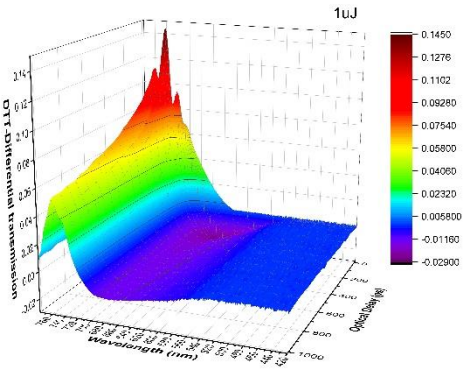

Figure 6: Differential transmission spectra of a pristine perovskite thin film at pump power of 1 μJ. Pump wavelength was set to 400 nm.

Then the differential transmission spectra were studied in encapsulated mini-modules before and after outdoor exposure. Figure 7 demonstrates the pump-probe spectra as collected on the initial date and after degradation. It is evident that the main characteristics i.e. position of the main peak (state filling) and differential transmission amplitude showed little change after this period of time.

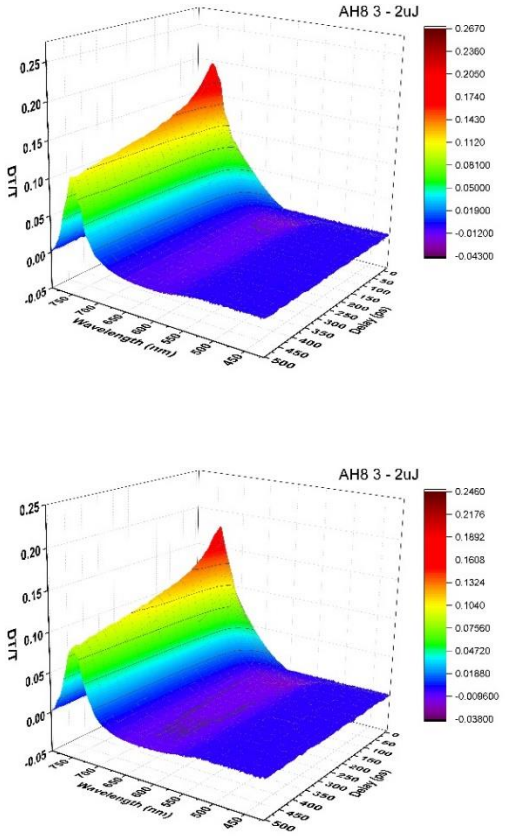

Figure 7: Pump-probe differential transmission data on sample labelled AH8 3 taken on (top) 29th July 2021 and (bottom) on 16th September 2021.

Further analysis of the ultrafast spectra was carried out to detect any differences in the decay constants. Table I presents the decay constants as derived by the exponential fittings on the main peak of the collected data. It is apparent that the degradation data revealed similar values for the peak wavelength and slight increase in relaxation times. This can be attributed to minor changes in the composition of the perovskite material. As changes in the chemical composition are becoming more significant the relaxation times obtained become noticeably increased.

Table I: Decay lifetimes before and after outdoor degradation as derived from pump probe measurements. Time constant have units of ps.

Sample	Before degradation (29/7/2021)	After degradation (16/9/2021)
AH8 3	y_0=0.54±0.01	y_0=0.49±0.01
	a_1=0.47±0.01	a_1=0.51±0.01
	τ_1=157.5±8.1	τ_1=191.5±11.4

3.5 Outdoor testing

After the microscopy and spectroscopy studies in perovskite thin films, six (6) encapsulated fully-functional devices with perovskite composition A and B have been monitored outdoors over the period from 12th of January until the 13th of May 2021 (16 weeks).

The normalized power conversion efficiency (PCE) over the sixteen weeks of outdoor exposure from all the 6 modules under test is depicted in Figure 8. Modules A1, A2, and A3 are of type A perovskite while modules B1, B2 and B3 are of type B perovskite. These measurements were taken at reverse sweeps and all parameters have been normalized to their initial values obtained outdoors. Over the entire period of exposure, type A modules presented higher PCE values than those of type B and this is attributed to the significant efficiency reduction of type B modules the first week of outdoor testing. The significant efficiency reduction in type B modules was found to be correlated to the open-circuit voltage loading between IV scans during outdoor exposure. This conclusion was found after indoor studies of both types of perovskites in the presence of Voc and MPP load [8]. Thus, even though the type B perovskites (thin film) demonstrated larger grains sizes in morphology and higher conductive currents when probed using microscopy methods, the outdoor behavior of those modules was significantly different from the results extracted in thin film level. The addition of extra layers (ETL, HTL etc.) in the full device adds more sources of degradation in devices and thus the behavior of the perovskite in a thin film level was shown to differ significantly compared to the perovskite in a full device.

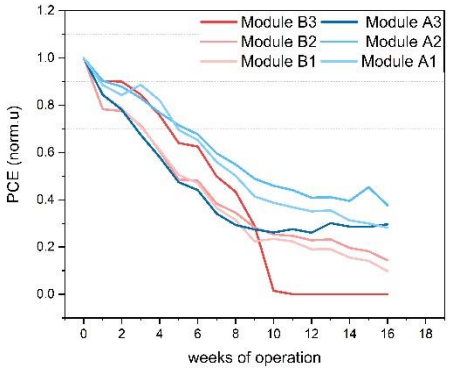

Figure 8: Weekly average performance (normalized values) of perovskites mini-modules of type A (A1, A2, A3) and B (B1, B2, B3) the first 16 weeks of outdoor exposure. Efficiency at reverse sweeps is reported on the graph.

4 CONCLUSIONS

In summary, several microscopic and spectroscopic techniques have been applied in bare and encapsulated thin film perovskite samples of two different perovskite compositions (labelled as type A and type B perovskites) and at different degradation stages (before and after their outdoor exposure). The SEM and AFM results showed different grain sizes and current densities at bare thin films. Perovskite thin films with additives (type B perovskite) exhibit larger grain size and less grain boundaries and therefore considerably higher current densities. However, during the outdoor exposure of full devices with type B perovskite composition, significant degradation was obtained due to the bias load applied and thus the beneficial effect of the additives was not detected. Therefore, the morphology results of thin perovskite films cannot be directly correlated with the outdoor behavior of full devices where all layers co-exist in the device.

Ultrafast spectroscopy was applied in only one type of perovskite (type A) before and after outdoor exposure. Pump-probe differential transmission data after degradation outdoors revealed slight changes in main peak position, differential transmission amplitude and carrier relaxation times.

5 AKNOWLEDGEMENTS

This work has been financed by the European Union through the TESTARE project (Grant ID: 101079488) and by the European Regional Development Fund and the Republic of Cyprus through the Cyprus Research and Innovation Foundation and the DegradationLab project (Grant ID: INFRASTRUCTURES/1216/0043).

6 REFERENCES

[1] C. A. Aranda, L. Caliò, and M. Salado,,Crystals 11 (2021) 1-16

[2] K. Domanski, E. Alharbi, A. Hagfeldt, M. Gratzel, and W. Tress, Nat. Energy 3 (2018) 61-67.

[3] M. Saliba *et al.*, Energy Environ. Sci., 9 (2016) 1989-1997

[4] C. S. Pathak, B. J. Chang, and S. Song, Dye. Pigment 218 (2023) 111469.

[5] A. Gomez, S. Sanchez, M. Campoy-Quiles, and A. Abate, Nano Energy 45 (2018) 94–100

[6] J. J. Li, J. Y. Ma, Q. Q. Ge, J. S. Hu, D. Wang, and L. J. Wan ACS Appl. Mater. Interfaces 7 (2015) 28518-28523.

[7] A. P. Thilakan *et al.*, ACS Appl. Mater. Interfaces 11 (2019) 21473-21480.

[8] V. Paraskeva *et al.*, Energies 16 (2023) 1-19.